

# Tetrazine molecules as efficient electronic diversion channel in 2D organic-inorganic perovskites

Ferdinand Lédée<sup>a,b</sup>, Pierre Audebert<sup>b\*</sup>, Gaëlle Trippé-Allard<sup>a</sup>, Laurent Galmiche<sup>b</sup>,  
Damien Garrot<sup>c</sup>, Jérôme Marrot<sup>d</sup>, Jean-Sébastien Lauret<sup>a</sup>, Emmanuelle Deleporte<sup>a\*</sup>,  
Claudine Katan<sup>e</sup>, Jacky Even<sup>f\*</sup>, Claudio Quarti<sup>e,g\*</sup>

<sup>a</sup> Université Paris-Saclay, ENS Paris-Saclay, CNRS, CentraleSupélec, LuMIn (Laboratoire Lumière, Matière et Interfaces), 91190 Gif-sur-Yvette, France.

<sup>b</sup> Université Paris-Saclay, ENS Paris-Saclay, CNRS, PPSM (Laboratoire de Photophysique et Photochimie Supramoléculaires et Macromoléculaires) - UMR 8531, 91190 Gif-sur-Yvette, France.

<sup>c</sup> Université Paris-Saclay, UVSQ, CNRS, GEMaC (Groupe d'étude de la Matière Condensée) – UMR 8635, 78000 Versailles, France.

<sup>d</sup> Université Paris-Saclay, UVSQ, CNRS, ILV (Institut Lavoisier de Versailles) - UMR 8180, 78000 Versailles, France.

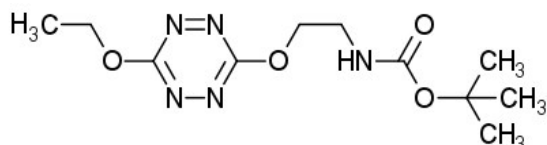
<sup>e</sup> Univ Rennes, ENSCR, INSA Rennes, CNRS, ISCR (Institut des Sciences Chimiques de Rennes) - UMR 6226, F 35000 Rennes, France.

<sup>f</sup> Univ Rennes, INSA Rennes, CNRS, Institut FOTON (Fonctions Optiques pour les Technologies de l'Information) - UMR 6082, 35000 Rennes, France.

<sup>g</sup> University of Mons, Laboratory for Chemistry of Novel Materials, B-7000 Mons, Belgium.

## Experimental section

### 1. Synthesis

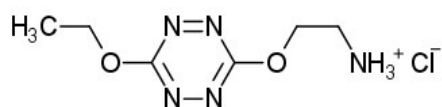


**2-(6-ethoxy-1,2,4,5-tetrazin-3-yl)oxyethyl-Boc-amine** : 3,6-Dichloro-1,2,4,5-tetrazine (97%, Sigma-Aldrich, 2.69 g, 18 mmol) was dissolved in 150 mL ethanol absolute (>99.9%, VWR Chemicals) and stirred overnight at room temperature. The solvent was then rotovated, and the precipitate was subsequently used without further purification. 1.73 g of the resulting 3-chloro-6-ethoxytetrazine was reacted with small excess of N-(tert-butoxycarbonyl)ethanolamine (98%, Sigma-Aldrich, 2 mL, 12.9 mmol) and 4-(dimethylamino)pyridine (DMAP) ( $\geq 99\%$  Sigma-Aldrich, 1.58 g, 12.9 mmol) in 150 mL anhydrous dichloromethane (DCM). The solution was continuously stirred at room temperature for 6 hours. The solvent was then rotovated and the pink precipitate purified by chromatography on silica gel (CH<sub>2</sub>Cl<sub>2</sub>/ethyl acetate). The <sup>1</sup>H NMR spectrum is shown in supplementary Fig. SX15. Yield: 50%.

<sup>1</sup>H NMR (300 MHz, CDCl<sub>3</sub>) :  $\delta$  (ppm) = 1.46 (s, 9H, 3x CH<sub>3</sub>), 1.56 (t,  $J$  = 7.0 Hz, 3H, CH<sub>3</sub>), 3.65 (q,  $J$  = 5.4 Hz, 2H, NCH<sub>2</sub>), 4.60 (t,  $J$  = 5.2 Hz, 2H, OCH<sub>2</sub>), 4.63 (q,  $J$  = 7.1 Hz, 2H, OCH<sub>2</sub>), 5.04 (s, 1H, NH).

<sup>13</sup>C NMR (300 MHz, CDCl<sub>3</sub>) :  $\delta$  (ppm) = 14.4 (CH<sub>3</sub>), 28.5 (3x CH<sub>3</sub>), 39.7 (CH<sub>2</sub>N), 66.1 (CH<sub>2</sub>O), 69.1 (CH<sub>2</sub>O), 155.9 (C=O), 80.0 (C(CH<sub>3</sub>)<sub>3</sub>), 166.3-166.0 (tetrazine core C<sub>sp2</sub>).

HRMS (ESI) : Expected 308.1335 Observed 308.1334



**2-(6-ethoxy-1,2,4,5-tetrazin-3-yl)oxyethylammonium chloride:** 900 mg of the previously synthesized 3-[2-hydroxy-(ethyl-N-Boc-amine)]-6-ethoxy-tetrazine were dissolved in 300 mL of anhydrous diethyl ether and reacted with gaseous hydrochloric acid (HCl) under vigorous stirring at room temperature. The gaseous chloric acid was obtained by carefully dropping a HCl solution (37% w/w, Aldrich,) on phosphoric anhydride powder ( $P_2O_5$ ). The cleavage of the Boc group and the protonation of the amine happened simultaneously without harming the tetrazine core. The ammonium salt was then recovered by filtration, rinsed with anhydrous diethyl ether and dried under vacuum. The salt was stored in a dessicator with  $P_2O_5$  for further use. The  $^1H$  NMR spectrum is shown in supplementary Fig. SX16. Yield: 64%.

$^1H$  NMR (500 MHz, DMSO- $D_6$ , 30°C) :  $\delta$  (ppm) = 1.41 (t,  $J$  = 7.1 Hz, 3H,  $CH_3$ ), 3.40 (t, 2H,  $NCH_2$ ), 4.53 (q,  $J$  = 7.2 Hz, 2H,  $OCH_2$ ), 4.68 (t,  $J$  = 5.2 Hz, 2H,  $OCH_2$ ), 8.18 (s, 3H,  $NH_3^+$ ).

$^{13}C$  NMR (500 MHz, DMSO- $D_6$ , 30°C) :  $\delta$  (ppm) = 14.7 ( $CH_3$ ), 38.4 ( $CH_2N$ ), 66.0 ( $CH_2O$ ), 66.1 ( $CH_2O$ ), 165.8-166.3 (tetrazine core  $C_{sp^2}$ ).

HRMS (ESI) : Expected 186.0991 Observed 186.0988

**Phenylethylammonium chloride:** phenylethylammonium salt was prepared by reacting 2-phenylethylamine (Aldrich, 99%) with a small excess of hydrochloric acid (37% w/w) in diethyl ether. The white precipitate was then filtered, dried in vacuum and stored in a dessicator with  $P_2O_5$  for further use.

## 2. X-Ray diffraction

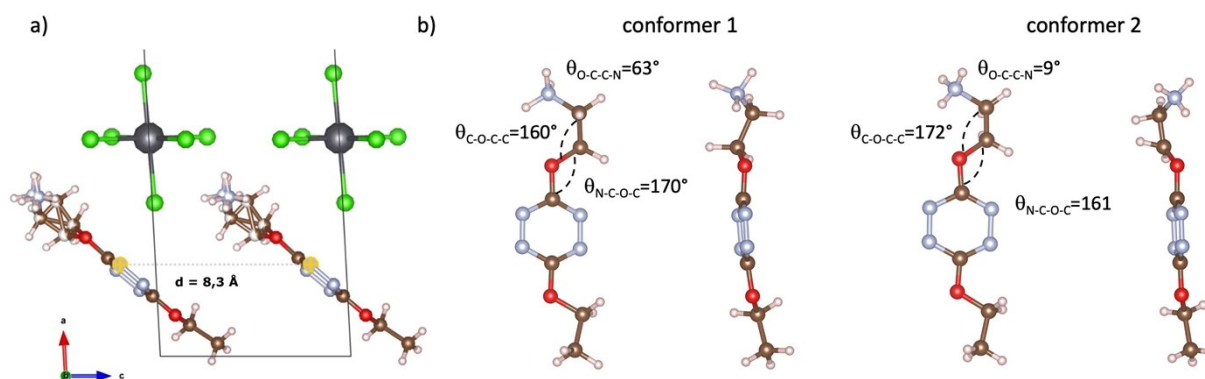


Figure SX1. a) Crystalline structure of  $Tz_2PbCl_4$  perovskite obtained from single crystal XRD measurement performed at 298 K. Distance between two aromatic cycles of Tz molecules in  $Tz_2PbCl_4$  is shown. b) Different conformers associated to 2-(6-ethoxy-1,2,4,5-tetrazin-3-yl)oxyethylammonium. Values assumed by dihedral angles ( $\theta$ ) are reported.

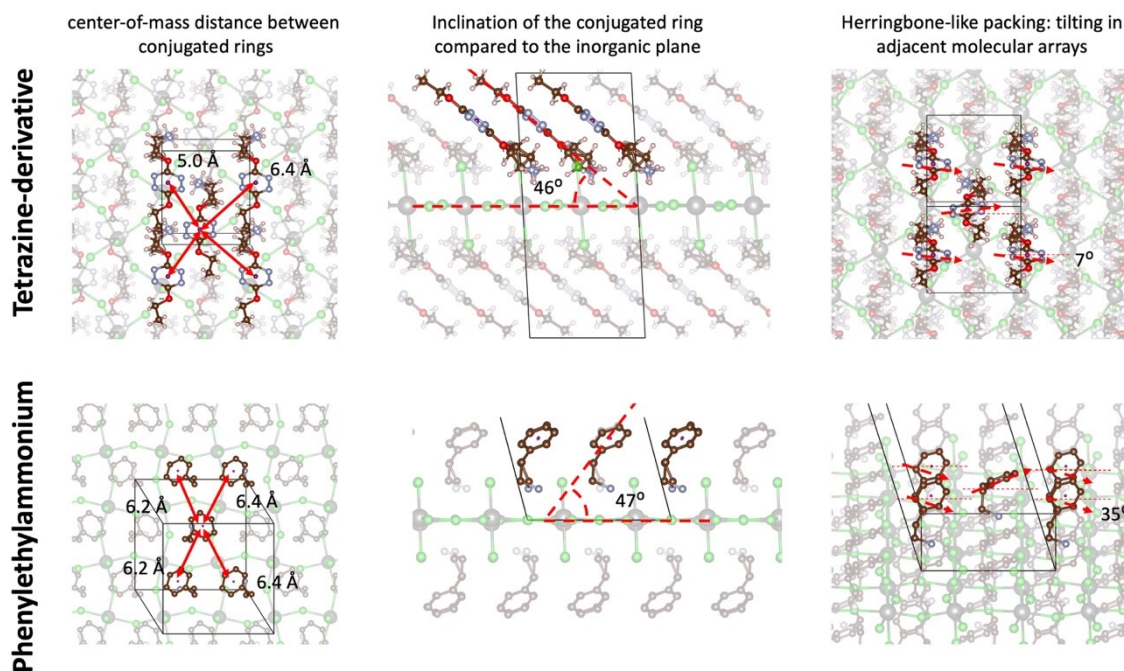
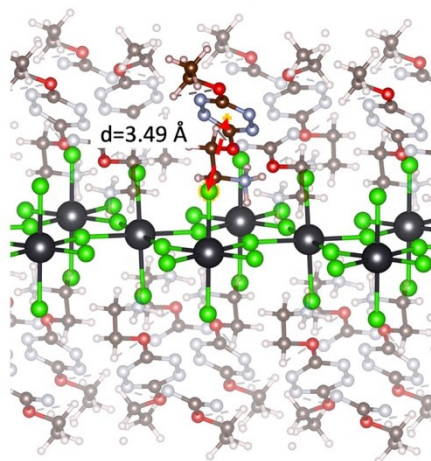


Figure SX2. Molecular packing of tetrazine-derivative spacer in our newly reported  $\text{PbCl}_4$  perovskite compound, as compared to that of phenylethylammonium, as reported in Ref<sup>1</sup>.

a) tetrazine derivative: this work



b) oligothiophene derivative: Nat. Chem. 11, 1151 (2019)

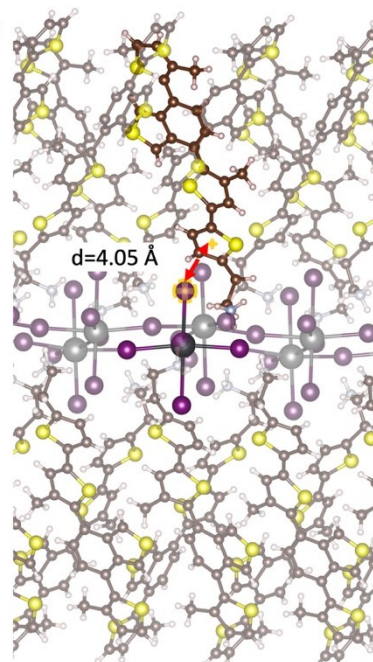


Figure SX3. Distance between the organic spacer and the inorganic  $\text{PbX}_4$  frame, as measured from the center of the  $\pi$ -conjugated ring and the closest halide in apical position. We compare the distance in the present compound to that measured in thiophene-incorporating  $\text{PbI}_4$  layered halide perovskite, reported by Dou and co-workers from Ref<sup>2</sup>, for which charge transfer from the inorganic frame to the organic component has been reported.

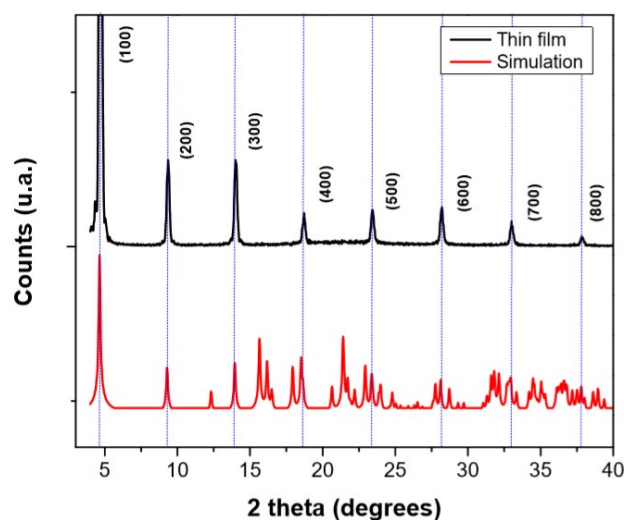


Figure SX4.  $Tz_2PbCl_4$  thin film diffraction diagram versus simulated diagram obtained from crystallographic data.

### 3. Photoluminescence

Table SX1. Optical properties of newly reported  $TzPbCl_4$  and  $TzPbCl_2Br_2$  compounds.

Compounds	Wannier $E_{1s}$ absorption (eV)	Wannier $E_{1s}$ PL (eV)	$E_{1s}$ PL FWHM (meV)	Tetrazine $S_2$ absorption (eV)	Tetrazine $S_1$ absorption (eV)	Tetrazine $S_1$ PL (eV)	$S_1$ PL FWHM (meV)
PEAPbCl <sub>4</sub>	3.64	3.60	68	-	-	-	-
PEAPbCl <sub>2</sub> Br <sub>2</sub>	3.36	3.23	216	-	-	-	-
$Tz_2PbCl_4$	3.68	-	-	3.45	2.37	2.20	300
$Tz_2PbCl_2Br_2$	3.35	-	-	3.4 – 3.5	2.37	2.20	280

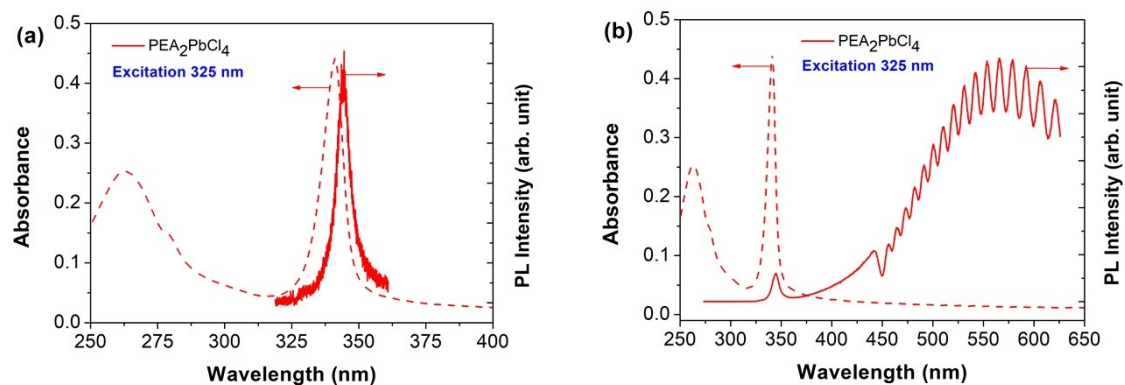


Figure SX5. (a-b) Photoluminescence (solid line) and Absorbance (dash line) spectra of a  $PEA_2PbCl_4$  thin film with two different monochromator grating. Oscillations seen in spectrum (b) are due to the transmission profile of the filter used to remove the 325 nm laser line.

## Oxidative electron transfer

It is very unlikely that the partial quenching of the luminescence of the tetrazines moieties inside the perovskite be due to oxidative electron transfer considering the standard redox potentials provided in the following discussion (values given vs SCE). First, the only possibility (according to the Nernst redox potentials) would be the chloride ion oxidation, since the  $\text{Pb}^{2+}/\text{Pb}^{4+}$  potential (+1.7 V) is higher than the one of the excited state of a dialkoxy tetrazine (estimation at + 1.65 V)<sup>3,4</sup>, without even considering the very high kinetic barrier for the transfer to the remote  $\text{Pb}^{2+}$  ion. The case of the chloride is more complicated, because, while the potential for the  $\text{Cl}^\ominus$  formation (+ 2.6 V) is very high, the reaction can be considerably driven down by the possible formation of chlorine  $\text{Cl}_2$ , which reduces the standard potential to +1.35 V. However, this is a multistep process whose values are measured in solution, unlikely to happen in a solid structure like a perovskite. Therefore, probably only the elemental electron transfer process needs to be taken into consideration; this additionally explains why even the mixed bromide perovskite is also unaffected, the  $\text{Br}^-/\text{Br}^\ominus$  potential being equal to 2.1 V.

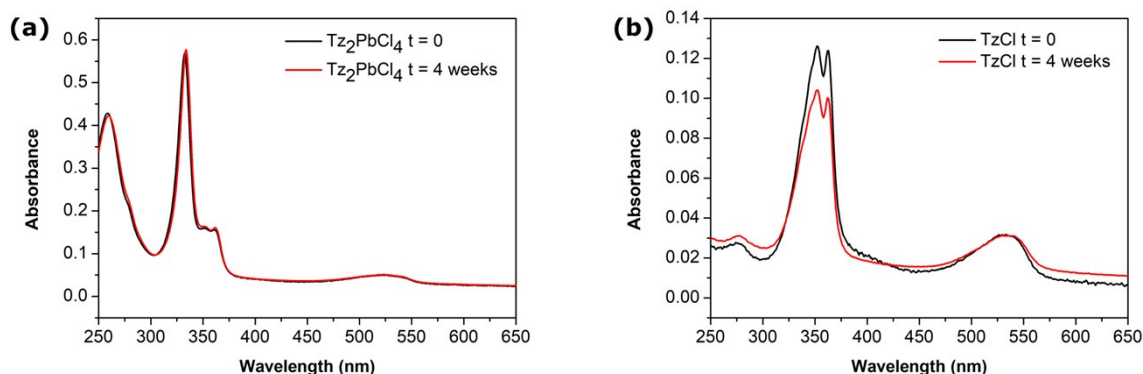


Figure SX6. Absorbance spectra of (a)  $\text{Tz}_2\text{PbCl}_4$  and (b)  $\text{TzCl}$  thin films at  $t = 0$  (black curves) and  $t = 4$  weeks (red curves).

## Electronic structure calculations

### 1. Simulation of the tetrazine excited states via Time Dependent-Density Functional Theory (TD-DFT) calculations:

Singlet and triplet excited states of functionalized 2-(6-ethoxy-1,2,4,5-tetrazin-3-yl)oxyethylammonium (Figure SX1-b) have been estimated using molecular simulations, adopting TD-DFT method. The computational approach is similar to the one proposed by Adamo et al.<sup>5</sup>, which provided accurate results for non-functionalised tetrazine (Figure SX7-a), in nice agreement with available experimental data and theoretical simulations from wavefunction based methods.<sup>6,7</sup> Standard PBE0 exchange-correlation functional (25% of exact exchange) was adopted, along with localized atomic basis set of triple split quality, 6-311G++(s,p), which includes diffuse and polarization functions. Calculations were performed using Gaussian16 program.<sup>8</sup>

Triplet and singlet excitation energies for non-functionalised tetrazine with D2h point group symmetry, as computed using our TD-DFT approach, are compared to wavefunction based methods in Figure SX7b.<sup>6,7</sup> There is a general agreement among the different computational methods in estimating the excited states energetics for the lowest two/three singlet/triplet excited states. Most notably, the energy difference between TD-DFT and wavefunction-based simulations for the second lowest lying triplet state is reduced, compared to the TD-DFT simulations for 2-(6-ethoxy-1,2,4,5-tetrazin-3-yl)oxyethylammonium, shown in Figure 4-a of the main text. This demonstrates that the difference between the computed energies is to be attributed to the nature of the molecule and not to the level of theory.

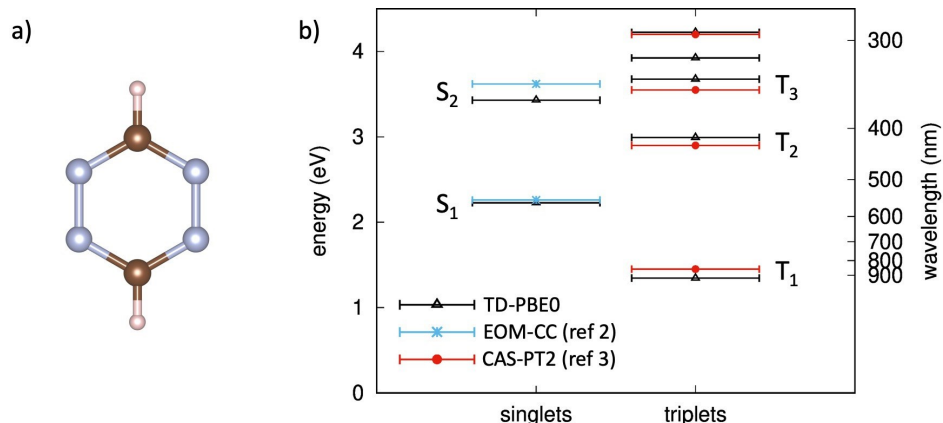


Figure SX7. a) Molecular structure for non-functionalized tetrazine; b) Singlet and Triplet excited states energies computed with TD-DFT for non-functionalized tetrazine, along with previous estimates based on wavefunction-based approaches (Equation Of Motion Coupled Cluster EOM-CC, ref <sup>6</sup> and Complete-Active-Space 2<sup>nd</sup> order Perturbation Theory, CAS-PT2, ref <sup>7</sup>).

## 2. Periodic Density Functional Theory (DFT) simulations of the bulk $Tz_2PbCl_4$ and $Tz_2PbCl_2Br_2$ perovskites:

Electronic structure calculations on bulk  $Tz_2PbCl_4$  and  $Tz_2PbCl_2Br_2$  perovskites are performed using periodic DFT method, in the planewave/pseudopotential formalism, as implemented in the pw.x program of the Quantum-Espresso Suite code.<sup>9,10</sup>

Crystalline models structures for pure chlorine, pure bromine, bromine-apical, bromine equatorial, bromine-random (Cl, Br, Br-ap, Br-eq, Br-rand, respectively) as defined in Figure 5a of the main text are fully optimized, relaxing both lattice parameters and atomic positions. Reference structure for pure chlorine compound, as obtained from XRD single crystal measurements, was affected by structural disorder in the site of the organic cation, with tetrazine having two possible conformers in the perovskite matrix (see Figure SX1b). We therefore performed preliminary calculations for this system to address the effect of the molecular conformation on the predicted electronic properties, finding negligible differences in the band gap and band dispersion. We therefore performed all the subsequent calculations considering the most stable crystalline structure, associated to conformer 1. To account for the effect of dispersive interactions among the organic Tz molecules on the final material structure, we adopted van-der-Waals Density Functional, vdw-DF2, developed by Langreth and Lundqvist,<sup>11</sup> along with ultrasoft pseudopotentials, 25 Ry/200Ry cutoff for the kinetic energy expansion of the wavefunction/electronic density and mesh of the indirect lattice of 4x4x2 (2 being the long interplanar axis) in the Monkhorst-Pack scheme.<sup>12</sup> The present method was shown to provide results for lead-iodide perovskites in nice agreement with respect to experimental data.<sup>13</sup> Computed equilibrium lattice parameters are reported in Table SX2.

Table SX2. Experimental lattice parameters for  $Tz_2PbCl_4$  and from DFT optimization (vdw-DF2 exchange-correlation functional), for the models investigated (see Figure 5-a): pure chlorine (Cl), bromine in apical position (Br-ap), bromine in equatorial position (Br-eq) and bromine randomly distributed (Br-rand). Difference between theory and experiment is reported in parenthesis.

		$a$ (Å)		$b$ (Å)		$c$ (Å)		$\beta$ (degrees)	
Cl	Expt	19.05		7.75		8.29		93.02	
	DFT	18.17	(-4.6%)	7.47	(-3.6%)	8.17	(-1.4%)	92.87	(-0.2%)
Br-ap	“	18.20		7.60		8.18		92.88	
Br-rand	“	18.18		7.56		8.21		92.88	
Br-eq	“	18.12		7.53		8.25		92.87	
Br	“	18.13		7.64		8.27		92.87	

Once the relaxed crystal structures are found, we investigate the electronic structure of the bulk materials. Quantitative prediction of the single particle electronic properties of lead halide perovskites is a complicated issue, as it requires to include both relativistic spin-orbit coupling<sup>14</sup> and accurate description of electronic exchange-correlation. We therefore employ here hybrid DFT calculations, based on PBE0 exchange correlation functional<sup>15</sup> with increased (30%) contribution of exact exchange, coupled with spin-orbit coupling. For these calculations, we resorted to norm-conserving pseudopotentials and 40 Ry/160 Ry cutoff for the planewave expansion of the wavefunction/electronic density. In light of the high computational cost of hybrid DFT calculations including spin-orbit coupling, we estimated the electronic structure only at the  $\Gamma$  point of the Brillouin zone, where the valence band maximum and conduction band minimum are located. Noteworthy, the present computational approach was shown to provide electronic bandgaps for layered hexylammonium and dodecylammonium lead iodide perovskites, in nice agreement with available experimental data.<sup>16</sup>

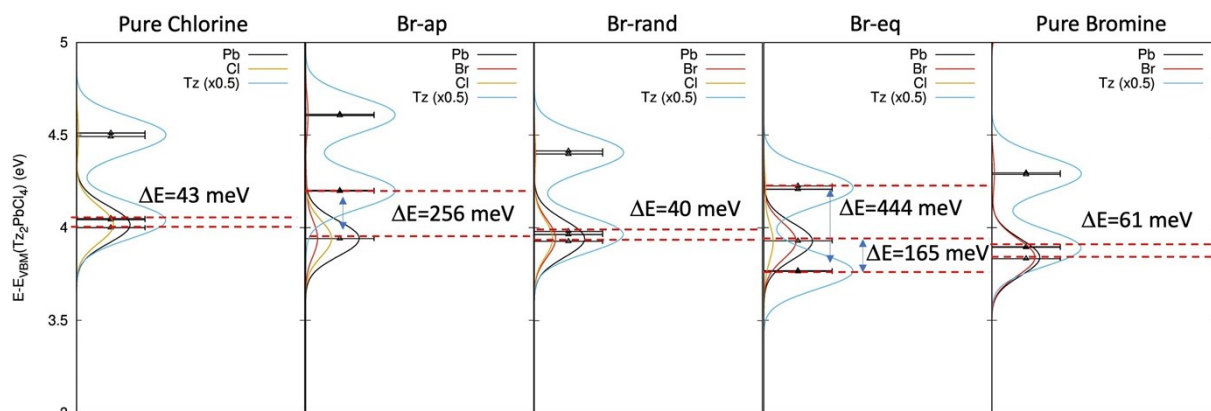


Figure SX8. Magnification of the atomic projected Density of State of the various perovskite models investigated, in the region of unoccupied lowest energy levels. Atomic contributions from the chlorine, bromine, lead and from the tetrazine are reported in orange, red, black and cyan, respectively. The contribution from tetrazine is halved, for graphical purposes.

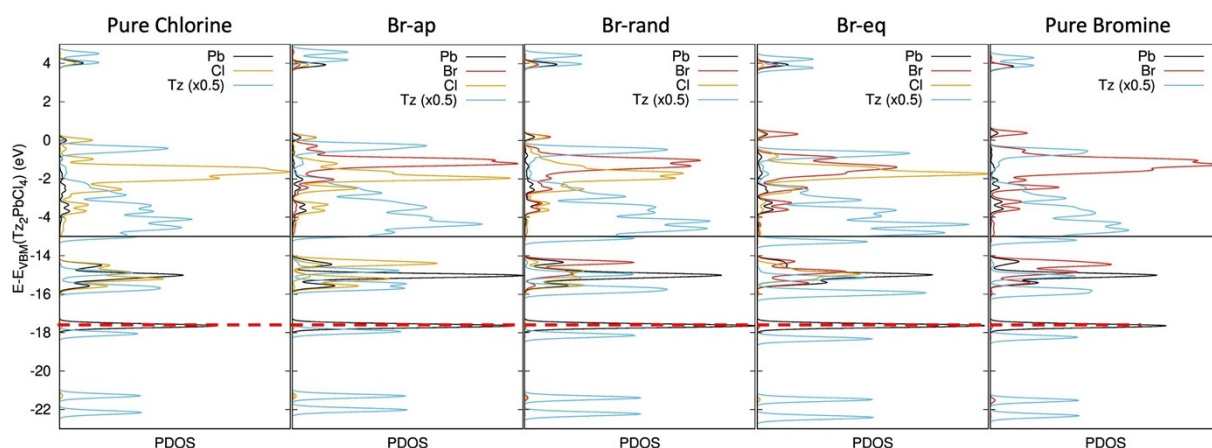


Figure SX9. Alignment of the electronic structure for the various tetrazine-based perovskite models. The valence band maximum of the chlorine compound was set to zero, as reference. Then, all the mixed chlorine/bromine and pure bromine models have been aligned with respect to the  $5d_{3/2}$  state of lead, as indicated by the dashed red line. Contributions from chlorine, bromine, lead and from the tetrazine are shown in orange, red, black and cyan. The contribution from tetrazine is halved, for graphical purposes.

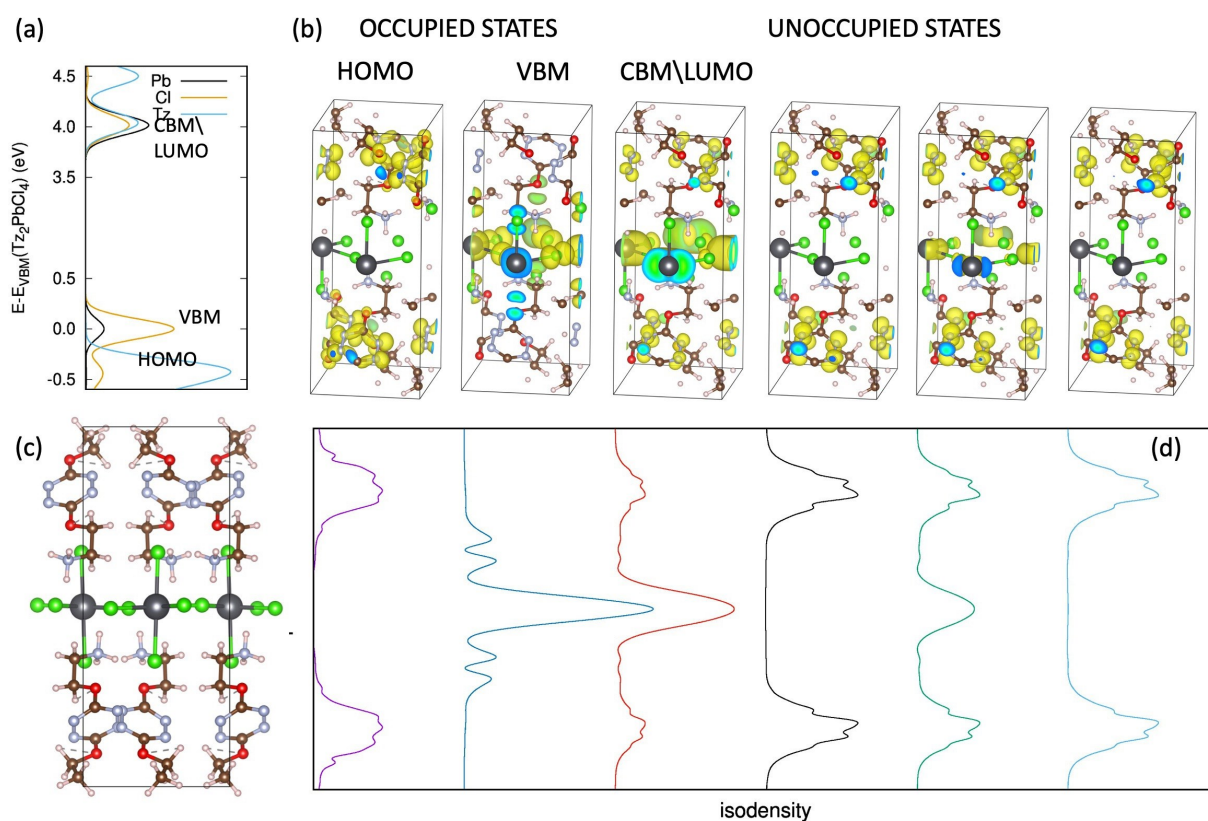


Figure SX10. Frontier orbitals for pure chlorine  $Tz_2PbCl_4$  model; (a) atomic projected Density of States in the region of the frontier orbitals, HOMO/LUMO and VBM/CBM. Valence Band Maximum (VBM) was taken as energy reference; (b) isodensity surfaces associated to the two highest energy occupied states and four lowest energy unoccupied states, as from hybrid PBE0+SOC calculations; (c) relaxed structure of pure chlorine  $Tz_2PbCl_4$  model; (d) planar average of the isodensities in (b), along the interplanar axis, highlighting the wavefunction localization on the central  $PbCl_4$  layer and/or on the Tz molecules.

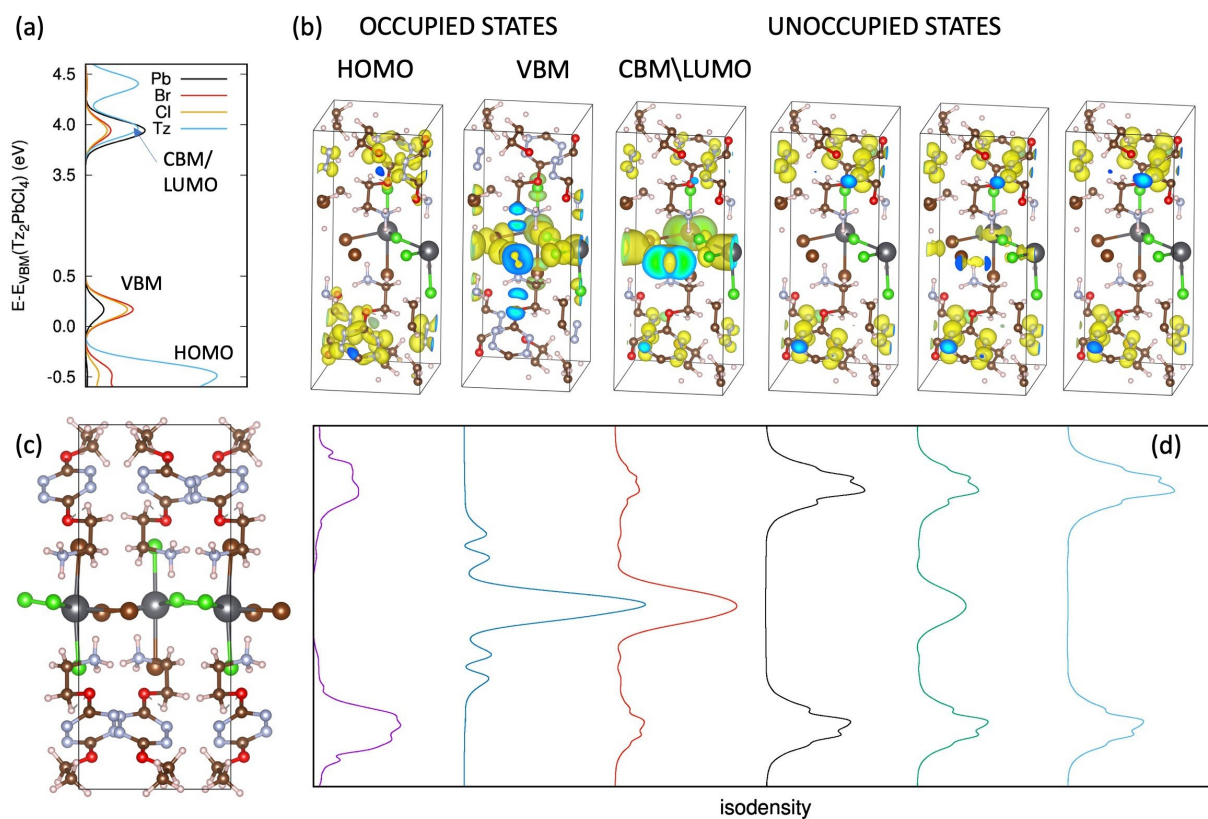


Figure SX11. Frontier orbitals for Br-rand  $Tz_2PbCl_2Br_2$  structure; (a) atomic projected Density of States in the region of the frontier orbitals, HOMO/LUMO and VBM/CBM. Valence Band Maximum (VBM) of  $Tz_2PbCl_4$  was taken as energy reference; (b) isodensity surfaces associated to the two highest energy occupied states and four lowest energy unoccupied states, as from hybrid PBE0+SOC calculations; (c) relaxed structure of Br-rand  $Tz_2PbCl_2Br_2$  model; (d) planar average of the isodensities in (b), along the interplanar axis, highlighting the wavefunction localization on the central  $PbX_4$  layer and/or on the Tz molecules.

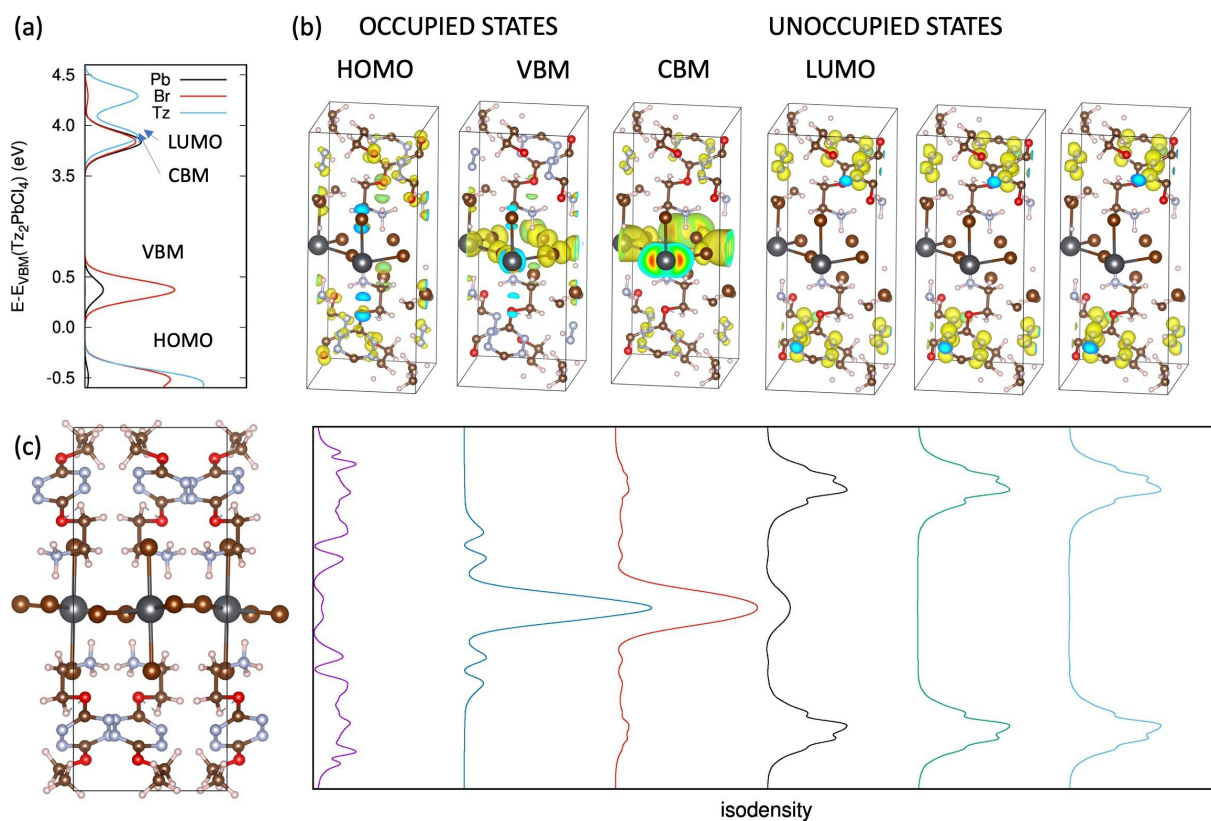


Figure SX12. Frontier orbitals for pure bromine  $\text{Tz}_2\text{PbBr}_4$  structure; (a) atomic projected Density of States in the region of the frontier orbitals, HOMO/LUMO and VBM/CBM. Valence Band Maximum (VBM) of  $\text{Tz}_2\text{PbCl}_4$  was taken as energy reference; (b) isodensity surfaces associated to the two highest energy occupied states and four lowest energy unoccupied states, as from hybrid PBE0+SOC calculations; (c) relaxed structure of pure  $\text{Tz}_2\text{PbBr}_4$  model; (d) planar average of the isodensities in (b), along the interplanar axis, highlighting the wavefunction localization on the central  $\text{PbBr}_4$  layer and/or on the Tz molecules.

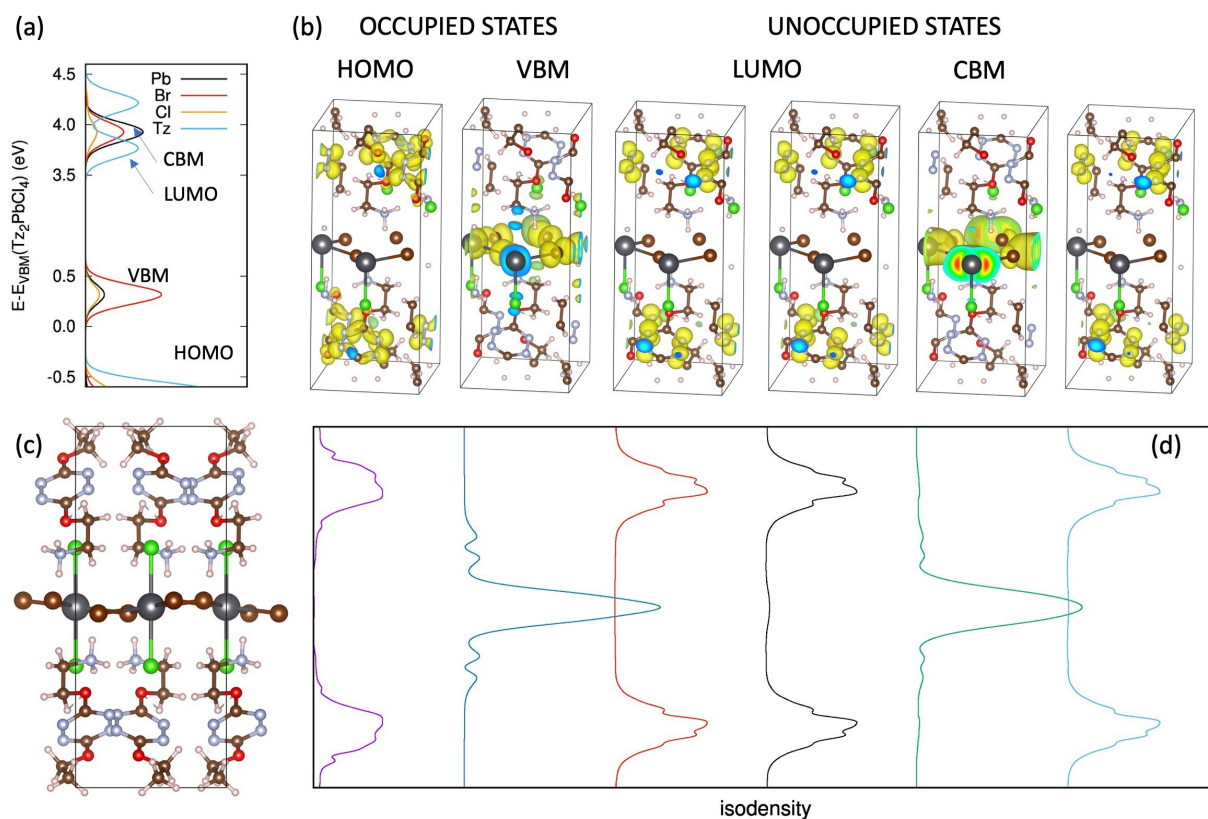


Figure SX13. Frontier orbitals for Br-eq  $Tz_2PbCl_2Br_2$  structure; (a) atomic projected Density of States in the region of the frontier orbitals, HOMO/LUMO and VBM/CBM. Valence Band Maximum (VBM) of  $Tz_2PbCl_4$  was taken as energy reference; (b) isodensity surfaces associated to the two highest energy occupied states and four lowest energy unoccupied states, as from hybrid PBE0+SOC calculations; (c) relaxed structure of Br-eq  $Tz_2PbCl_2Br_2$  model; (d) planar average of the isodensities in (b), along the interplanar axis, highlighting the wavefunction localization on the central  $PbX_4$  layer and/or on the Tz molecules.

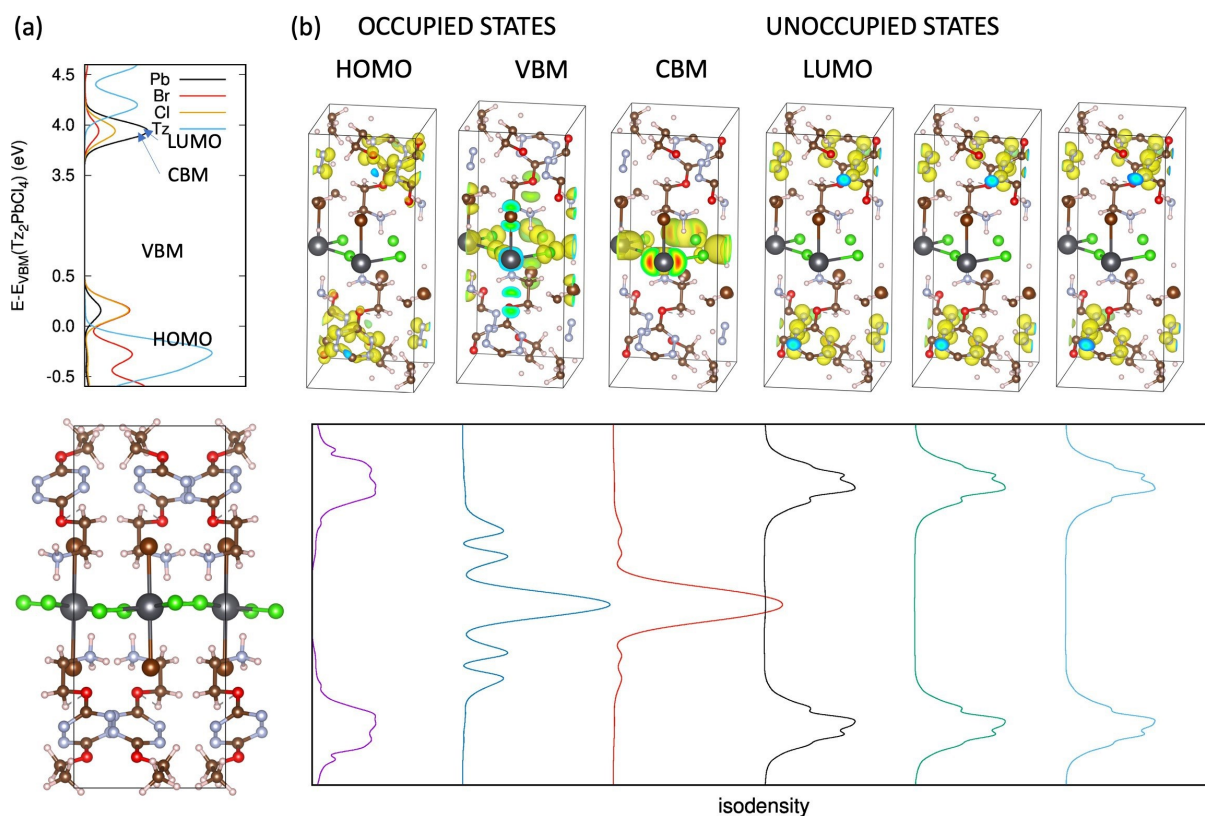


Figure SX14. Frontier orbitals for Br-ap  $Tz_2PbCl_2Br_2$  structure; (a) atomic projected Density of States in the region of the frontier orbitals, HOMO/LUMO and VBM/CBM. Valence Band Maximum (VBM) of  $Tz_2PbCl_4$  was taken as energy reference; (b) isodensity surfaces associated to the two highest energy occupied states and four lowest energy unoccupied states, as from hybrid PBE0+SOC calculations; (c) relaxed structure of Br-ap  $Tz_2PbCl_2Br_2$  model; (d) planar average of the isodensities in (b), along the interplanar axis, highlighting the wavefunction localization on the central  $PbX_4$  layer and/or on the Tz molecules.

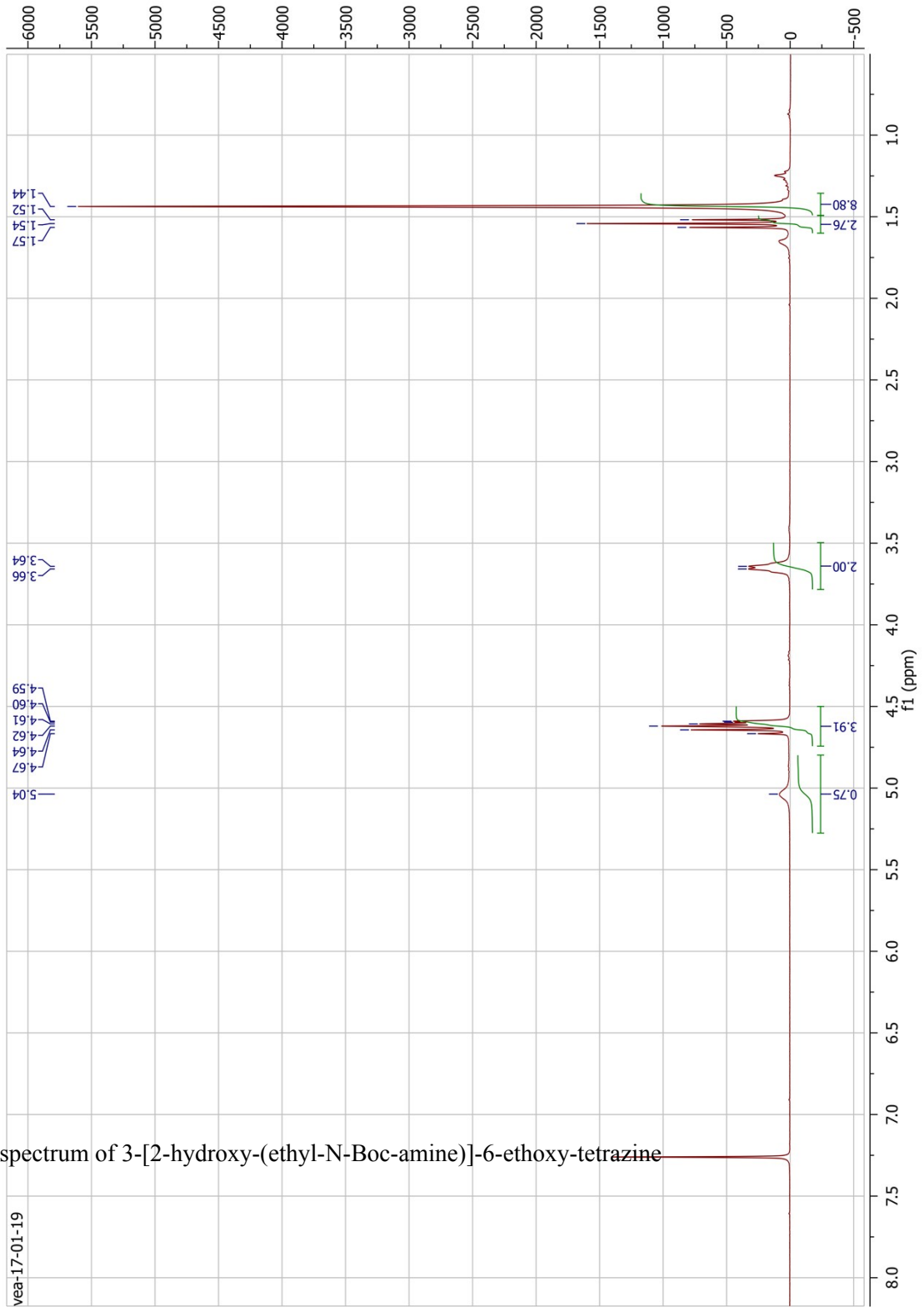


Figure SX15.  $^1\text{H}$  NMR spectrum of 3-[2-hydroxy-(ethyl-N-Boc-amine)]-6-ethoxy-tetrazine

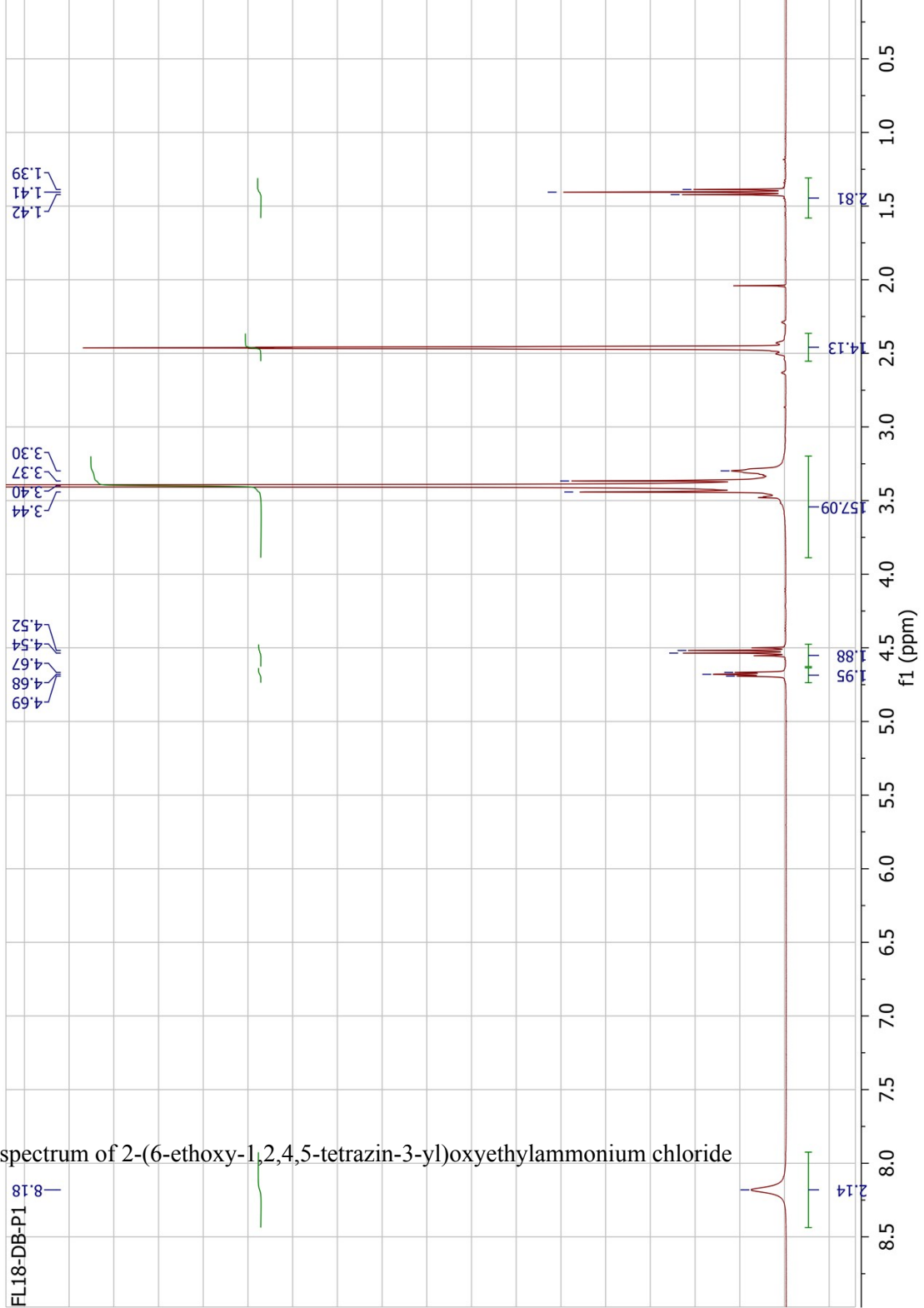


Figure SX16.  $^1\text{H}$  NMR spectrum of 2-(6-ethoxy-1,2,4,5-tetrazin-3-yl)oxyethylammonium chloride

## References

- 1 D. B. Mitzi, *J. Solid State Chem.*, 1999, **145**, 694–704.
- 2 Y. Gao, E. Shi, S. Deng, S. B. Shiring, J. M. Snaider, C. Liang, B. Yuan, R. Song, S. M. Janke, A. Liebman-Peláez, P. Yoo, M. Zeller, B. W. Boudouris, P. Liao, C. Zhu, V. Blum, Y. Yu, B. M. Savoie, L. Huang and L. Dou, *Nat. Chem.*, 2019, **11**, 1151–1157.
- 3 P. Audebert, F. Miomandre, G. Clavier, M.-C. Vernières, S. Badré and R. Méallet-Renault, *Chem. Eur. J.*, 2005, **11**, 5667–5673.
- 4 G. Clavier and P. Audebert, *Chem. Rev.*, 2010, **110**, 3299–3314.
- 5 C. Adamo and V. Barone, *Chem. Phys. Lett.*, 2000, **330**, 152–160.
- 6 M. Nooijen, *J. Phys. Chem. A*, 2000, **104**, 4553–4561.
- 7 M. Rubio and B. O. Roos, *Molecular Physics*, 1999, **96**, 603–615.
- 8 M. J. Frisch, G. W. Trucks, H. B. Schlegel, G. E. Scuseria, M. A. Robb, J. R. Cheeseman, G. Scalmani, V. Barone, G. A. Petersson, H. Nakatsuji, X. Li, M. Caricato, A. V. Marenich, J. Bloino, B. G. Janesko, R. Gomperts, B. Mennucci, H. P. Hratchian, J. V. Ortiz, A. F. Izmaylov, J. L. Sonnenberg, Williams, F. Ding, F. Lipparini, F. Egidi, J. Goings, B. Peng, A. Petrone, T. Henderson, D. Ranasinghe, V. G. Zakrzewski, J. Gao, N. Rega, G. Zheng, W. Liang, M. Hada, M. Ehara, K. Toyota, R. Fukuda, J. Hasegawa, M. Ishida, T. Nakajima, Y. Honda, O. Kitao, H. Nakai, T. Vreven, K. Throssell, J. A. Montgomery Jr., J. E. Peralta, F. Ogliaro, M. J. Bearpark, J. J. Heyd, E. N. Brothers, K. N. Kudin, V. N. Staroverov, T. A. Keith, R. Kobayashi, J. Normand, K. Raghavachari, A. P. Rendell, J. C. Burant, S. S. Iyengar, J. Tomasi, M. Cossi, J. M. Millam, M. Klene, C. Adamo, R. Cammi, J. W. Ochterski, R. L. Martin, K. Morokuma, O. Farkas, J. B. Foresman and D. J. Fox, *Gaussian 16 Rev. C.01*, Wallingford, CT, 2016.
- 9 P. Giannozzi, S. Baroni, N. Bonini, M. Calandra, R. Car, C. Cavazzoni, D. Ceresoli, G. L. Chiarotti, M. Cococcioni, I. Dabo, A. D. Corso, S. de Gironcoli, S. Fabris, G. Fratesi, R. Gebauer, U. Gerstmann, C. Gougoussis, A. Kokalj, M. Lazzeri, L. Martin-Samos, N. Marzari, F. Mauri, R. Mazzarello, S. Paolini, A. Pasquarello, L. Paulatto, C. Sbraccia, S. Scandolo, G. Sclauzero, A. P. Seitsonen, A. Smogunov, P. Umari and R. M. Wentzcovitch, *J. Phys.: Condens. Matter*, 2009, **21**, 395502.
- 10 P. Giannozzi, O. Andreussi, T. Brumme, O. Bunau, M. B. Nardelli, M. Calandra, R. Car, C. Cavazzoni, D. Ceresoli, M. Cococcioni, N. Colonna, I. Carnimeo, A. D. Corso, S. de Gironcoli, P. Delugas, R. A. DiStasio, A. Ferretti, A. Floris, G. Fratesi, G. Fugallo, R. Gebauer, U. Gerstmann, F. Giustino, T. Gorni, J. Jia, M. Kawamura, H.-Y. Ko, A. Kokalj, E. Küçükbenli, M. Lazzeri, M. Marsili, N. Marzari, F. Mauri, N. L. Nguyen, H.-V. Nguyen, A. Otero-de-la-Roza, L. Paulatto, S. Poncé, D. Rocca, R. Sabatini, B. Santra, M. Schlipf, A. P. Seitsonen, A. Smogunov, I. Timrov, T. Thonhauser, P. Umari, N. Vast, X. Wu and S. Baroni, *J. Phys.: Condens. Matter*, 2017, **29**, 465901.
- 11 K. Lee, É. D. Murray, L. Kong, B. I. Lundqvist and D. C. Langreth, *Phys. Rev. B*, 2010, **82**, 081101.
- 12 H. J. Monkhorst and J. D. Pack, *Phys. Rev. B*, 1976, **13**, 5188–5192.
- 13 I. García-Benito, C. Quarti, V. I. E. Queloz, S. Orlandi, I. Zimmermann, M. Cavazzini, A. Lesch, S. Marras, D. Beljonne, G. Pozzi, M. K. Nazeeruddin and G. Grancini, *Chem. Mater.*, 2018, **30**, 8211–8220.
- 14 J. Even, L. Pedesseau, J.-M. Jancu and C. Katan, *J. Phys. Chem. Lett.*, 2013, **4**, 2999–3005.
- 15 C. Adamo and V. Barone, *J. Chem. Phys.*, 1999, **110**, 6158–6170.
- 16 C. Quarti, N. Marchal and D. Beljonne, *J. Phys. Chem. Lett.*, 2018, **9**, 3416–3424.